Supplementary Information (SI) for Dalton Transactions.

Electronic Supplementary Material (ESI)

for

Optimization of Fe(III) Based Negative Electrodes for Lithium-ion Batteries: Probing Electrochemical Performance and Stability Characteristics

Tushar Singh,[a†] Ghanshyam Varshney,[b†] Shivali Hans,[c] Srijan Sengupta,[b,d]* Subrata Chakraborty[a.d]*

[a]Department of Chemistry, Indian Institute of Technology Jodhpur, Karwar, Jodhpur, 342037, Rajasthan, India.

[b]Department of Metallurgical and Materials Engineering, Indian Institute of Technology Jodhpur, Karwar, Jodhpur, 342037, Rajasthan, India.

[c]Department of Chemistry, School of Sciences, Cluster University of Jammu, Canal Road, Jammu, 180001, Jammu and Kashmir, India.

[d]Rishabh Centre for Research and Innovation in Clean Energy, Indian Institute of Technology Jodhpur, Karwar, Jodhpur, 342037, Rajasthan, India.

***Correspondence:** Dr. Srijan Sengupta, srijansengupta@iitj.ac.in and Dr. Subrata Chakraborty, subrata@iitj.ac.in

[†]These authors contributed equally to this work and share first authorship.

Table of Contents

EXPERIMENTAL SECTION

Methods and Materials

Air and moisture-sensitive reactions and experiments were carried out under nitrogen or argon atmosphere using standard Schlenk techniques or glove box. Dry solvents were obtained using the standard solvent purification method or purchased from Sigma Aldrich. Unless otherwise noted, all commercially available compounds were purchased from Sigma Aldrich, Tokyo Chemical Industry Co., Ltd. (TCI) Chemicals, Spectrochem Pvt. Ltd., and BLD Pharmatech (India) Pvt. Ltd. (BLD pharma), Chempure Pvt. Ltd. and used as received without further purification. All the solvents for routine isolation of products and chromatography were laboratory reagent grade and distilled before use. Analytical thin-layer chromatography (TLC) was performed on the TLC Silica Gel 60 F254 Aluminium Sheets (MERCK), and UV light (254 nm) was used for the visualization.

Instrumentation

Multinuclear NMR data were obtained froma Bruker High Performance, 500 MHz, and tetramethylsilane (TMS) as the internal standard was used. High resolution mass spectra

(HRMS) were recorded on a Waters Xevo Q-TOF Mass Spectrometer using the electrospray ionization (ESI) technique. UV−vis and FT-IR spectroscopic measurements were performed on Varian Carry 400 and Bruker Vertex 70 V+PMA50 instruments. SEM-EDS studies were performed on an SEM-Carl Zeiss EVO 18 instrument. XPS analysis was performed on a high-resolution X-ray photoelectron spectrometer (Physical Electronics, PHI 5000 VersaProbe III). A TGA-6000 thermal analyzer (PerkinElmer) was used to record TGA. The cyclic voltammetry of the complexes was measured in 0.1 M NBu_4PF_6 acetonitrile solutions under a nitrogen atmosphere. A three-electrode configuration (Pt working electrode, Pt wire counter electrode, and Ag/AgCl reference electrode) and a PC-controlled using a CH Instruments electrochemical analyzer. Accordingly, $E_{1/2}$ of the Fc^+/Fc (Fc = ferrocene) couple under the experimental condition was 0.41 V. The controlled electrochemical experiments were conducted on a CHI6154E potentiostat under an oxygen-free atmosphere. The aqueous electrolytic solution was degassed with the purging of nitrogen gas for at least 30 min for all the experiments. All electrochemical datawere corrected with *iR* (ohmic potential drop) losses arising from the solution resistance unless specifically mentioned.

PHYSIOCHEMICAL CHARACTERIZATION OF COMPLEX C-1

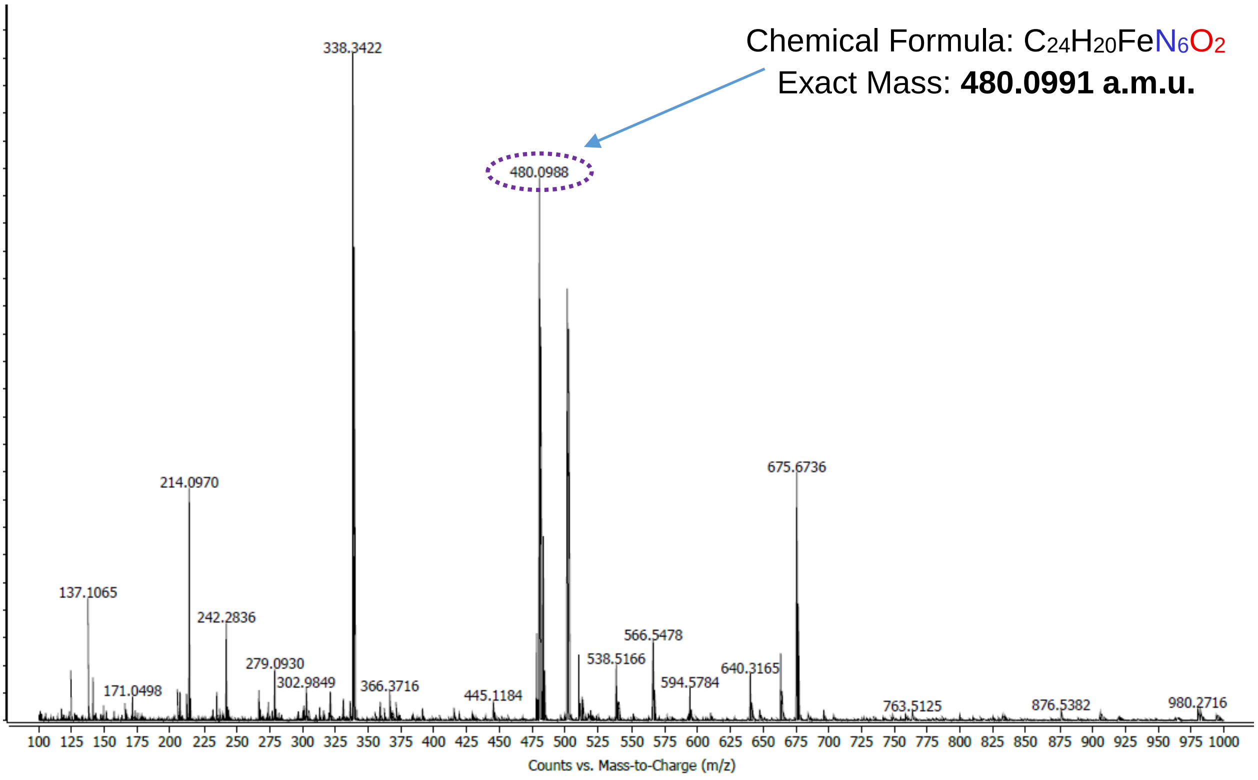

Chemical Formula: $C_{24}H_{20}FeN_6O_2$
Exact Mass: **480.0991 a.m.u.**

Figure S1. HRMS of the complex **C-1**.

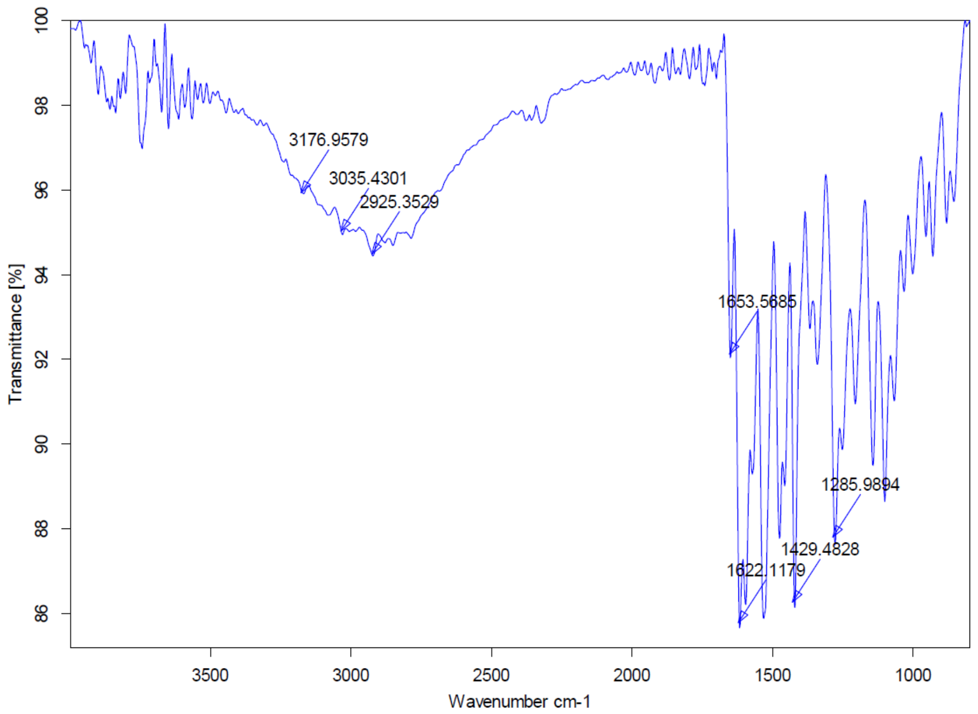

Figure S2. IR spectrum for the complex **C-1**.

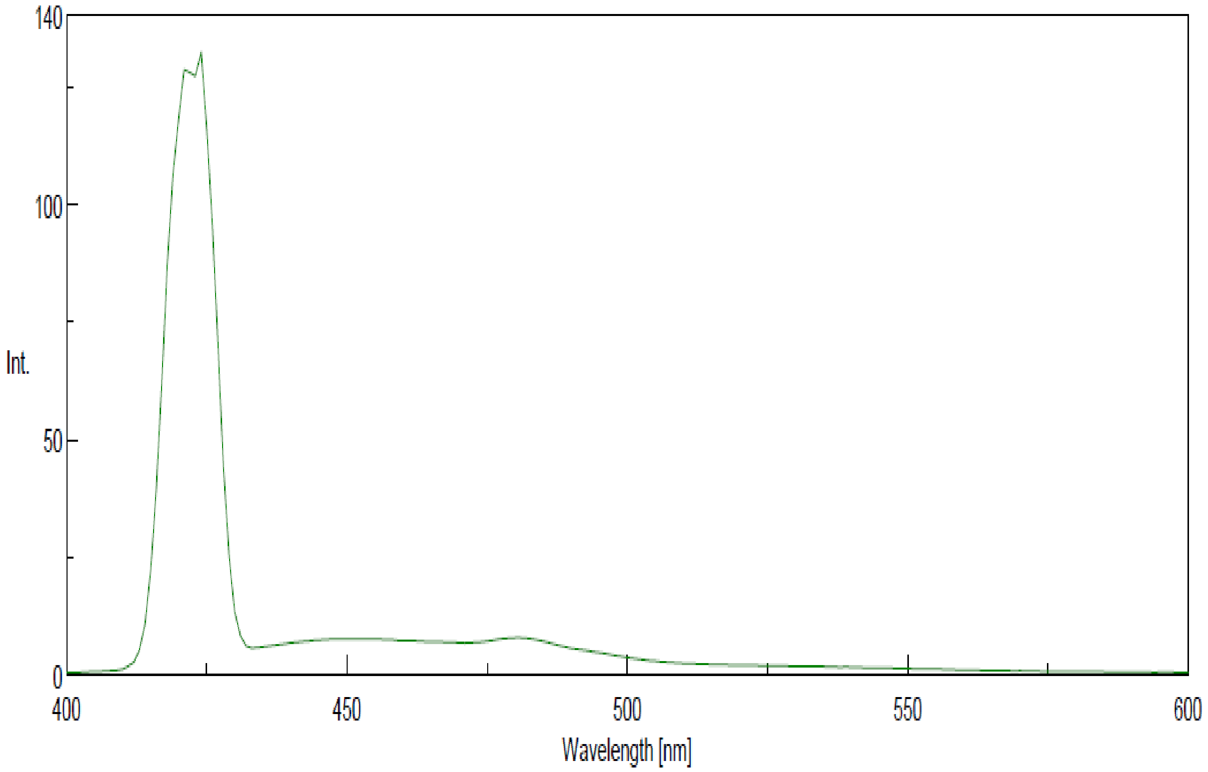

Figure S3. Emission spectrum of **C-1** in methanol recorded at 298 K excited at 390 nm.

THERMAL STABILITY OF COMPLEX C-1

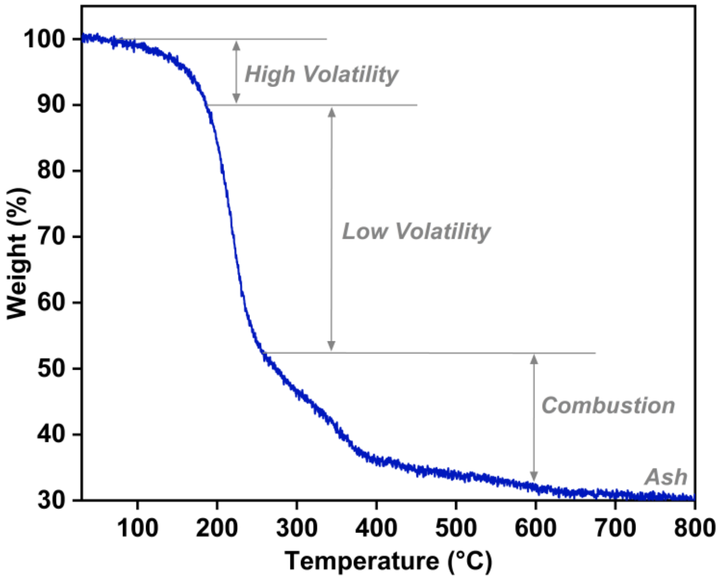

Figure S4. TGA plot of **C-1**.

The thermogravimetric analysis (TGA) curve of **C-1** indicates the elimination of the moisture or volatile solvent at temperatures ranging from 100 to 200 °C. Gradual weight loss is observed from (200-400)°C, which could correspond to stepwise removal of the ligands from the complex. However, major decomposition is observed in the temperature range of 400°C to 800°C. Hence, the catalyst is stable upto 200 °C (Figure **S4**).

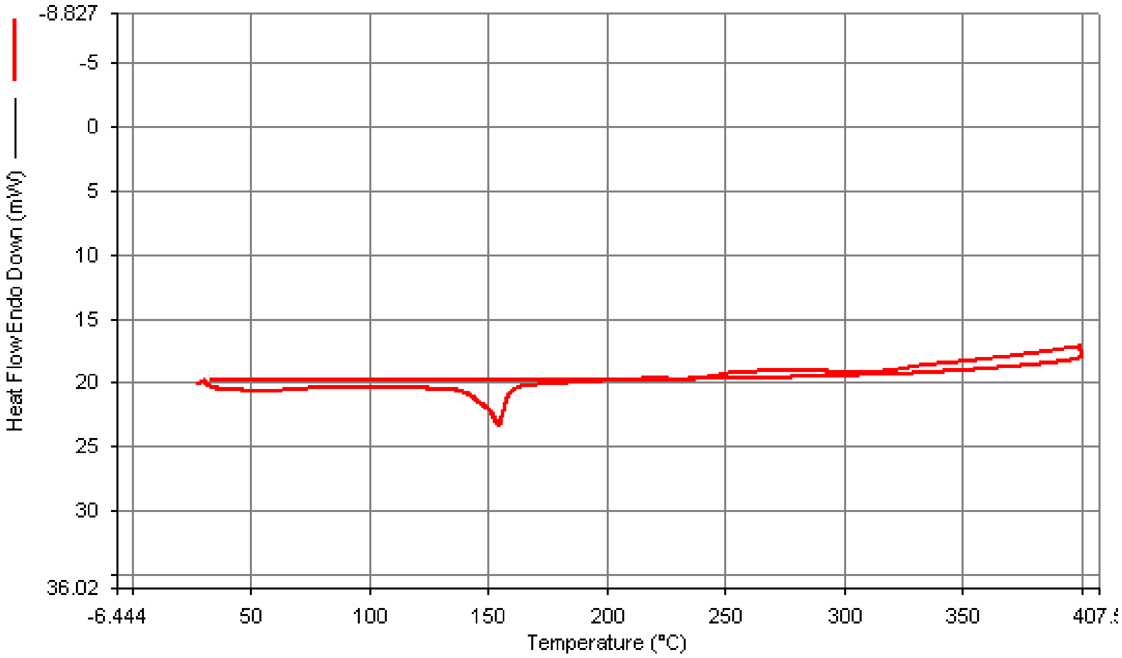

Figure S5. DSC plot of **C-1**.

From the differential scanning calorimetry (DSC) plot, upto ~400°C, the curve shows relative stability with gradual downward trend. However, after 400°C, significant heat absorption is observed suggesting a phase transition such as melting. (Figure **S5**).

COMPUTATIONAL DETAILS OF COMPLEX C-1

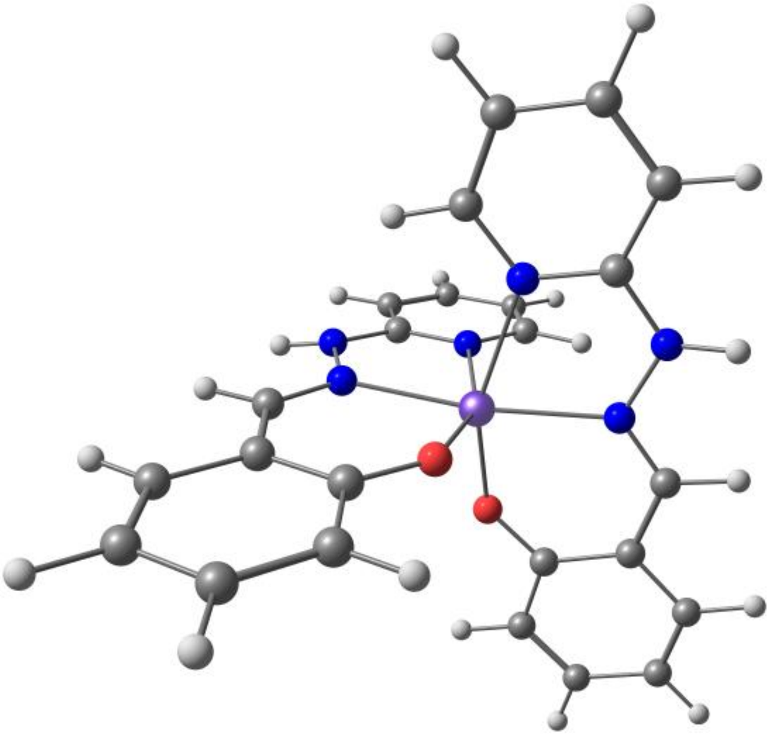

Optimized geometry

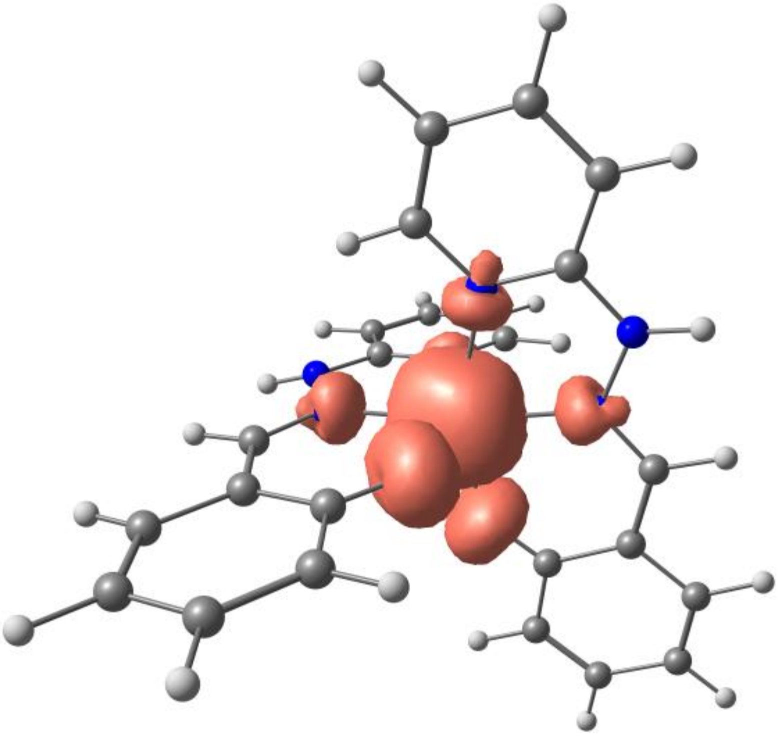

Spin density (*iso-surface value = 0.005*)

Figure S6. Optimized geometry and spin density plot of **C-1**.

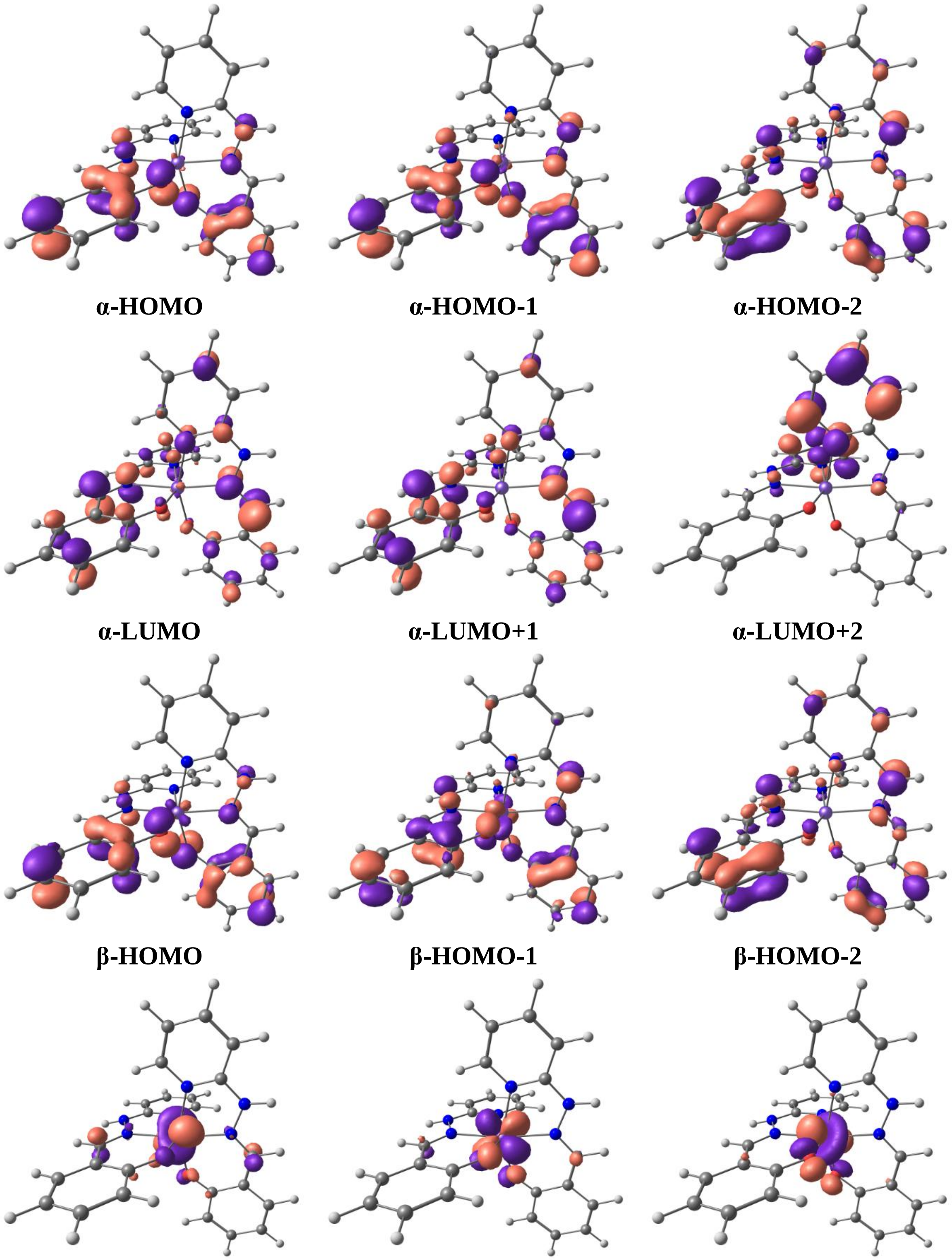

α-HOMO **α-HOMO-1** **α-HOMO-2**

α-LUMO **α-LUMO+1** **α-LUMO+2**

β-HOMO **β-HOMO-1** **β-HOMO-2**

β-LUMO **β-LUMO+1** **β-LUMO+2**

Figure S7: Frontier Molecular orbital diagram(s) of complex **C-1** *(iso-surface value = 0.05)*.

Table S1. XYZ coordinates of the DFT optimized structure of complex **C-1**

Center Number	Atomic Number	Atomic Type	Coordinates (Angstroms) X	Y	Z
1	26	0	-0.001151	-0.044788	-0.000800
2	8	0	-1.311784	1.181288	-0.640585
3	8	0	1.301445	1.193378	0.632197
4	7	0	0.843158	-1.628326	1.286362
5	7	0	-0.936906	-1.124135	2.670413
6	1	0	-1.316518	-1.042708	3.606541
7	7	0	-1.316820	-0.199889	1.722423
8	7	0	-0.836562	-1.638819	-1.280153
9	7	0	0.944631	-1.136872	-2.663645
10	1	0	1.324573	-1.058395	-3.599952
11	7	0	1.318830	-0.205029	-1.720644
12	6	0	1.980686	-2.308954	1.028205
13	1	0	2.431118	-2.116828	0.059960
14	6	0	2.550871	-3.188482	1.929522
15	1	0	3.465536	-3.712542	1.680070
16	6	0	1.915419	-3.370898	3.168638
17	1	0	2.334699	-4.048057	3.905980
18	6	0	0.748945	-2.683378	3.452383
19	1	0	0.233742	-2.806247	4.399311
20	6	0	0.237515	-1.812298	2.472690
21	6	0	-2.368730	0.529330	1.976314
22	1	0	-2.880103	0.381505	2.933122
23	6	0	-2.930091	1.513375	1.104003
24	6	0	-4.080701	2.216080	1.539725
25	1	0	-4.487685	1.994066	2.523222
26	6	0	-4.682833	3.168066	0.740475
27	1	0	-5.562258	3.699951	1.086298
28	6	0	-4.139807	3.440602	-0.529671
29	1	0	-4.607730	4.188672	-1.163020
30	6	0	-3.015110	2.772635	-0.986950
31	1	0	-2.591096	2.982093	-1.963096
32	6	0	-2.379404	1.797974	-0.186861
33	6	0	-1.972496	-2.321420	-1.020221
34	1	0	-2.425359	-2.125168	-0.053930
35	6	0	-2.538279	-3.207784	-1.917614
36	1	0	-3.451806	-3.733233	-1.666917
37	6	0	-1.899953	-3.395204	-3.154496
38	1	0	-2.315788	-4.077768	-3.888799
39	6	0	-0.735066	-2.705680	-3.439978
40	1	0	-0.217749	-2.832287	-4.385258
41	6	0	-0.228159	-1.827527	-2.464288
42	6	0	2.369296	0.525602	-1.976343
43	1	0	2.883974	0.372864	-2.930608
44	6	0	2.925140	1.517145	-1.108986
45	6	0	4.075319	2.219894	-1.545750

```
    46          1           0        4.486284    1.992029   -2.526249
    47          6           0        4.672152    3.179127   -0.751191
    48          1           0        5.551346    3.710920   -1.097744
    49          6           0        4.123980    3.459211    0.515092
    50          1           0        4.587691    4.213023    1.144720
    51          6           0        2.999451    2.791510    0.973182
    52          1           0        2.571423    3.006817    1.946299
    53          6           0        2.369190    1.809399    0.177896
 ---------------------------------------------------------------------
```

SOAKING TEST EVALUATION

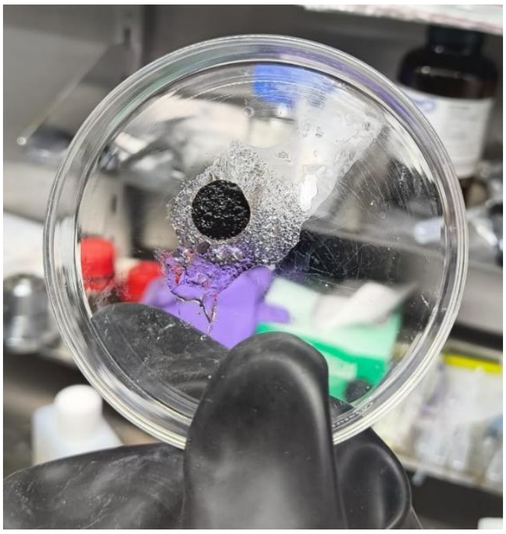

Figure S8. Soak test evaluation of the Fe-based molecular complex tape-casted electrode in organic electrolyte.

The photographic evidence obtained after the soaking period presented here clearly shows that the electrode coating was visually intact with no visible delamination, swelling, discolouration, or physical degradation of the active material layer. The typical deep black appearance of the C-1 electrode coating was fully maintained after soaking, with no leaching or surface degradation of the material. Furthermore, no measurable change in the weight of the electrode was found before and after the soaking test through gravimetric measurements, excluding the possibility of the tape-casted material dissolving into the electrolyte. No colouration or turbidity was observed in the electrolyte solution during the soaking period, indicating that no material dissolved. The electrolyte solution remained optically clear.

- No visible change in electrode coating appearance
- No measurable weight loss before and after soaking
- Electrolyte remained optically clear, no coloration or turbidity

The soaking test, photographic evidence and corresponding gravimetric data have been incorporated into the revised manuscript to substantiate the long-term stability claims of the Fe-based molecular complex electrode.

CYCLIC VOLTAMMETRY MEASUREMENT AT DIFFERENT SCAN RATES:

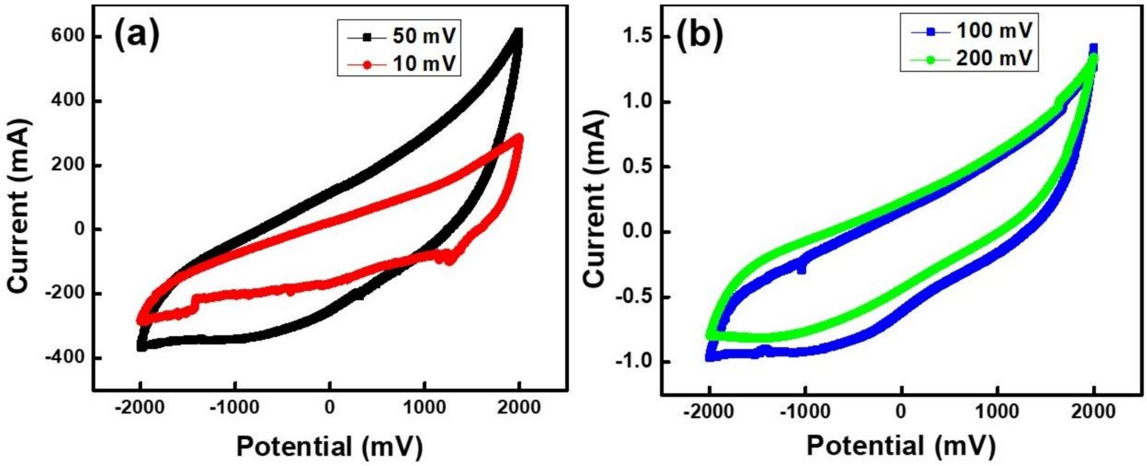

Figure S9. Cyclic voltammograms of the C-1 electrode recorded over a potential window of (−2000 to +2000) mV at scan rates of (**a**) 10 and 50 mV s^{-1} and (**b**) 100 and 200 mV s^{-1}, illustrating the scan rate-dependent current response and the predominantly capacitive charge storage behavior of the electrode.

The electrochemical charge storage performance of the C-1 electrode was studied by Cyclic Voltammetry (CV) in the potential range of −2000 to +2000 mV at different scan rates (Figure **S9**). At low scan rates (10 and 50 mV s^{-1}), Figure **S9**(**a**), the CV profiles are broad and quasi-rectangular, lacking sharp, well-defined redox peaks. This suggests that the charge storage mechanism is primarily capacitive, with potential diffusion-controlled contributions, as evidenced by the slight deviation from the ideal rectangular shape. The progressive increase of enclosed area with increase in scan rate from 10 to 50 mV s^{-1} confirms the current response depending on scan rate.

At higher scan rates of 100 and 200 mV s^{-1}, Figure **S9**(**b**) the CV curves maintain their characteristic quasi-rectangular shape with good symmetry between the anodic and cathodic sweeps, indicating excellent electrochemical reversibility and fast ion transport kinetics at the electrode-electrolyte interface. The pseudocapacitive nature of charge storage in the **C-1** electrode is confirmed by the shape retention at all scan rates without much distortion, and its ability for efficient charge delivery even at high-rate conditions.

The apparent difference in current magnitude between Figure S9(a) and Figure S9(b) is a result of the fact that these two measurements were performed on two different coin cells of the same mass loading, where slight differences in electrode surface contact, electrolyte wetting, and internal resistance led to the difference in absolute current values observed.